applied sciences

MDPI

Article

First-Principles Prediction of Skyrmionic Phase Behavior in $GdFe_2$ Films Capped by 4*d* and 5*d* Transition Metals

Soyoung Jekal [1,2,*], Andreas Danilo [3], Dao Phuong [4] and Xiao Zheng [4]

1 Laboratory of Metal Physics and Technology, Department of Materials, ETH Zurich, 8093 Zurich, Switzerland
2 Condensed Matter Theory Group, Paul Scherrer Institute, CH-5232 Villigen PSI, Switzerland
3 Laboratory for Solid State Physics, Department of Physics, ETH Zurich, 8093 Zurich, Switzerland; a.danilo@gmail.com
4 Hefei National Laboratory, University of Science and Technology of China, Hefei 230026, Anhui, China; d.phuong@gmail.com (D.P.); xiaozz@gmail.com (X.Z.)
* Correspondence: so-young.jekal@mat.ethz.ch; Tel.: +41-44-632-26-43

Received: 22 January 2019; Accepted: 8 February 2019; Published: 13 February 2019

Abstract: In atomic $GdFe_2$ films capped by 4*d* and 5*d* transition metals, we show that skyrmions with diameters smaller than 12 nm can emerge. The Dzyaloshinskii–Moriya interaction (DMI), exchange energy, and the magnetocrystalline anisotropy (MCA) energy were investigated based on density functional theory. Since DMI and MCA are caused by spin–orbit coupling (SOC), they are increased with 5*d* capping layers which exhibit strong SOC strength. We discover a skyrmion phase by using atomistic spin dynamic simulations at small magnetic fields of ∼1 T. In addition, a ground state that a spin spiral phase is remained even at zero magnetic field for both films with 4*d* and 5*d* capping layers.

Keywords: skyrmion; Dzyaloshinskii–Moriya interaction; exchange energy; magnetic anisotropy

1. Introduction

In the sphere of magnetic memory storage (especially in spintronics), magnetic skyrmions, which are localized topologically protected spin structures, are promising candidates due to their unique properties [1–3]. Even though skyrmions have long been investigated by simulations such as micromagnetic and phenomenological model calculations [4–6], the experimental discovery of skyrmions was came about very recently in bulk MnSi [7]. Since then, researchers have focused on observing stabilized skyrmions experimentally in not only bulk crystals [8,9], but also thin films and multilayers [10–14].

At room temperature, Neél-type skyrmions with a diameter of ∼50 nm are found in multilayer stacks, such as Pt/Co/Ta and Ir/Fe/Co/Pt [15,16]. However, to use them in memory and logic devices, a further reduction in skyrmion sizes is necessary. As a result of the decreasing stability of small skyrmions at room temperature, thicker magnetic layers are required to increase stability [17,18]. For multilayer systems consisting of ferromagnet and heavy metals, interfacial anisotropy and the strength of Dzyaloshinskii–Moriya interaction (DMI) reduces as the thickness of ferromagnetic layer increases. Moreover, the skyrmion Hall effect is a challenge when it comes to moving skyrmions in electronics devices [19–21]. Amorphous rare-earth–transition-metal (RE–TM) ferrimagnets are one of the potential materials to overcome these challenges. Their Intrinsic perpendicular magnetocrystalline anisotropy (MCA) gives an advantage in stabilizing skyrmions by using relatively thick magnetic layers (∼5 nm) [22]. Another advantage of RE–TM alloys is that the skyrmion Hall effect is largely reduced by the near zero magnetization of RE–TM alloys [23]. Furthermore, in perspective of the

applications, all-optical helicity-dependent switching (AO-HDS) has been shown in RE–TM alloys due to its ultrafast switching. Recently, AO-HDS has been demonstrated in RE–TM alloys using a circularly polarized laser. As a result, RE–TM alloys have drawn interest in the field of skyrmions research.

In recent, large skyrmions with diameter of ∼150 nm have been observed in Pt/GdFeCo/MgO [24], and skyrmion bound pairs are found in Gd/Fe multilayers [25]. However, further tuning is essential to reduce the size of skyrmions in RE–TM alloys.

In the present paper, magnetic properties such as DMI, MCA, and magnetic phase transition are investigated in atomic $GdFe_2$ films capped by 4*d* and 5*d* transition metals (TMs) using first principles density functional theory (DFT) calculations and atomistic spin dynamics simulations. We recognize that the 5*d* TMs give rise to a large DMI and strong MCA due to their large spin–orbit coupling (SOC) and orbital hybridization with 3*d* bands of Fe atom. Firstly, an extended Heisenberg model is studied by using atomistic spin dynamics. Then, we parameterize an extended Heisenberg model from DFT calculations. According to the phase diagram observed at zero temperature, there are phase transitions under externally applied magnetic fields of the order of ∼1 T. The magnetic phase changes from the spin spiral state to the ferromagnetic state via skyrmion lattice, the diameters of isolated skyrmions amount to 6 to 15 nm depending on the capping layers.

2. Methods

We used DFT as implemented in the Quantum Espresso [26] and Fleur code [27] to investigate the electronic and magnetic properties of $GdFe_2$/TMs film. For the TMs capping layers, we have considered Ru, Rh, Pd, and Ag in 4*d* and Os, Ir, Pt and Au in 5*d*. For the exchange–correlation potential we adapted the generalized gradient approximation (GGA). The wave functions were expanded by a plane-wave basis set with an optimized cutoff energy of 350 Ry, and the Brillouin zone was sampled via a $12 \times 12 \times 1$ *k*-point mesh. Different mesh values from 36 to 256 were tested to ensure the precision of our calculations, with the convergence criterion being 0.1 μeV. The convergence with respect to cutoff was also carefully checked.

Total energy E(q) is calculated along the paths of $\bar{\Gamma}$-$\bar{K}$ and $\bar{\Gamma}$-$\bar{M}$ which have the highest symmetry among other directions in the two-dimensional Brillouin zone (2D BZ). E(q) with and without SOC [28] are separately displayed in Figure 1. In the 2D BZ, we characterize spin spiral phase using the wave vector **q** with a constant angle of ϕ, where ϕ is defined as $\mathbf{q}\cdot\mathbf{R}$.

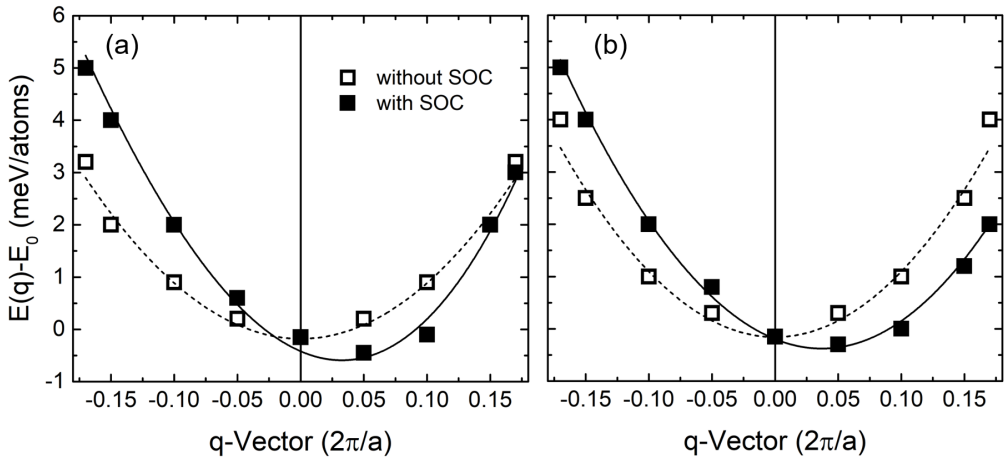

Figure 1. Energy dispersion E(q) of homogeneous cycloidal flat spin spirals in high-symmetry direction $\bar{\Gamma}$-$\bar{K}$ for (**a**) $GdFe_2$/Rh and (**b**) $GdFe_2$/Rh films. Filled and empty symbols represent E(q) with and without SOC, respectively. The energy is given relative to the magnetic ground state. The dispersion is fitted to the Heisenberg model (dotted line) and includes the DMI and MCA (solid line).

In order to examine the magnetically characteristic of $GdFe_2$ films with TM capping layers, we adopt the atomistic spin model given by References [29–31]:

$$H = -\sum_{ij} J_{ij}(m_i \cdot m_j) - \sum_{ij} D_{ij}(m_i \times m_j) + \sum_i K(m_i^z)^2 - \sum_i \mu_s(B \cdot m_i). \quad (1)$$

By using Equation (1), we can describe the magnetic interactions between two neighbor Fe atoms with spins of $\mathbf{M}_i$ and $\mathbf{M}_j$ at sites $\mathbf{R}_i$ and $\mathbf{R}_j$, respectively. Here, m_i is defined as $\mathbf{M}_i/\mu_s$. Both energy dispersion curves (with and without SOC) are calculated and fitted to extract the parameters for the exchange interactions (J_{ij}) and the DMI (D_{ij}).

We then compute the magnetic state by solving the Landau–Lifshitz–Gilbert (LLG) equation,

$$\frac{d\mathbf{S}_i}{dt} = -\gamma' \mathbf{S}_i \times (\mathbf{B}_i^{\text{eff}} + \mathbf{B}_i^{\text{th}}) - \gamma' \alpha \mathbf{S}_i \times [\mathbf{S}_i \times (\mathbf{B}_i^{\text{eff}} + \mathbf{B}_i^{\text{th}})]. \quad (2)$$

Here α denotes the Gilbert damping parameter. When γ is the gyromagnetic ratio, γ' represents $\frac{\gamma}{1+\alpha^2}$. $\mathbf{B}_i^{\text{eff}}$ is the effective magnetic field at site i, and $\mathbf{B}_i^{\text{th}}$ is the thermal noise. The LLG simulations were done with mumax3 [32]. For the present systems we use material parameters obtained from DFT: K = 2–14 meV and D = 0.2–1.6 meV (see Figure 2). To verify the numerical stability of the simulations, calculations with different cell sizes were performed. Finally, the thin films are discretized in a 400 × 400 × 2 mesh with periodic boundary conditions in in-plane directions.

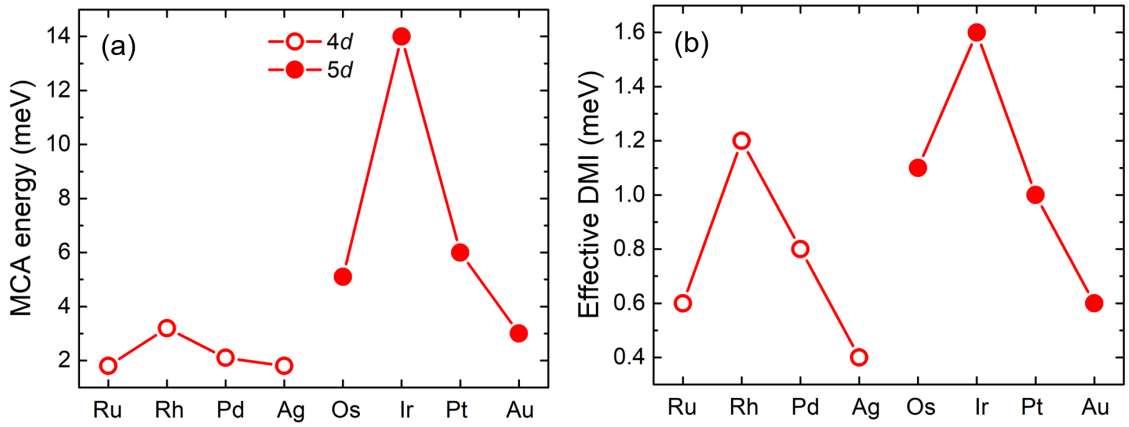

Figure 2. (**a**) Total magnetocrystalline anisotropy (MCA) energy and (**b**) effective Dzyaloshinskii–Moriya interaction (DMI) of $GdFe_2$ with TM capping layer.

The MCA energy was calculated using the force theorem and defined as the total energy difference between the magnetization perpendicular to the [100]-plane and parallel to the [100]-plane. Therefore, MCA energy $E_{\text{MCA}} = \text{E}_{[100]} - E_{[001]}$, where $E_{[100]}$ and $E_{[001]}$ are the total energies with the magnetization aligned along the [100] and [001] of the magnetic anisotropy, respectively.

3. Results and Discussion

The in-plane lattice constant of 7.32 Å was taken from the experimental lattice constant of Laves phase of $GdFe_2$, with lattice mismatches of 3.6% (Rh)–14.2% (Os), as depicted in Figure 3a. From the total energy calculation, it was confirmed that the hollow site is the most energetically favorable to stack the TM layer (see Figure 3). The atoms of $GdFe_2$ and TM capping layer were fully relaxed by atomic force calculations.

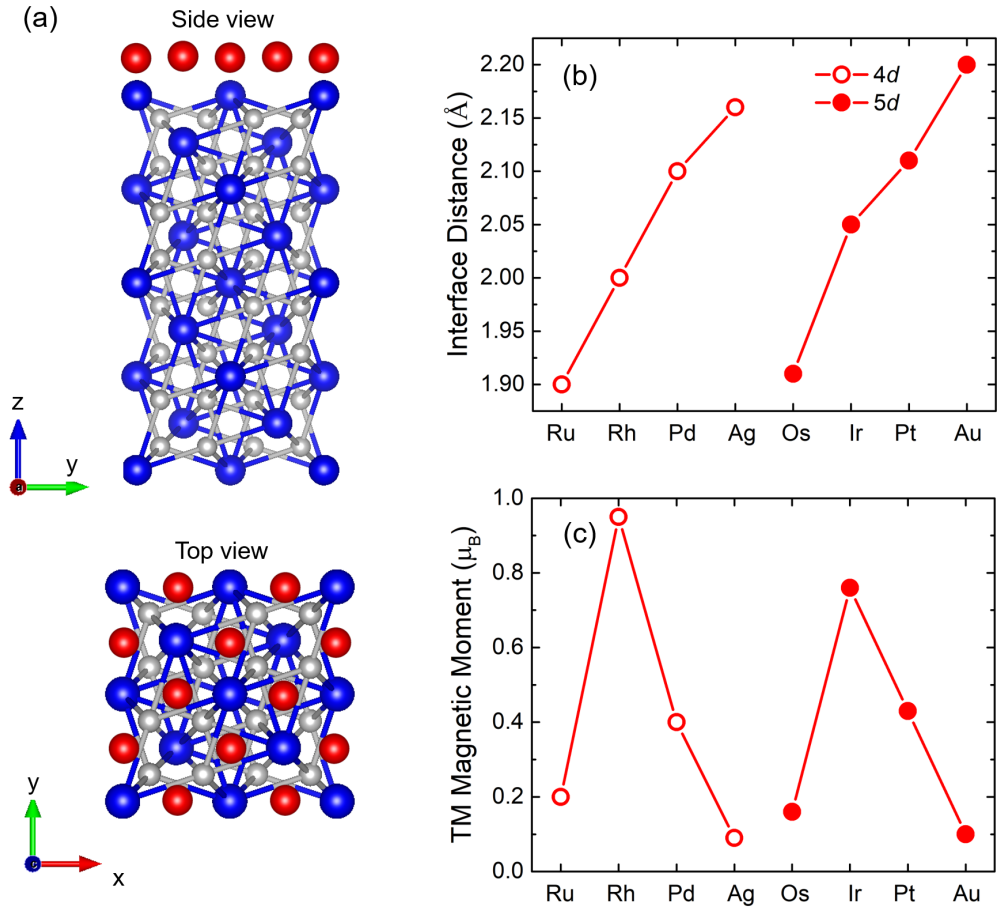

Figure 3. (**a**) Side view and top view of $GeFe_2$ film capped by a transition-metal (TM) monolayer. Blue, gray, and red balls represent Gd, Fe, and TM atoms, respectively. TM atoms are on the hollow site of $GeFe_2$; (**b**) Interface distances between the TM capping layer and $GeFe_2$ after structural optimization; (**c**) Magnetic moments of TM atoms, induced by $GeFe_2$.

After structural optimization, the interface distances between the TM capping layer and the $GdFe_2$ is presented in Figure 3b. As the atomic number becomes larger in the 4*d* and 5*d* TMs , the interlayer distances increase monotonically. Induced spin moments of the TMs for TM/$GdFe_2$ are presented in Figure 3c. The Rh and Ir capping layers, which are the Co-group elements, are found to have the largest moments of 0.98 and 0.80 μ_B. For all of the TM/$GdFe_2$, the direction of magnetization is favored to perpendicularly orientate to the film plane. Interestingly, the MCA energy and DMI of $GdFe_2$ films capped by 5*d* TMs are significantly larger than those of $GdFe_2$ with 4*d* TMs. In particular, the Ir-capped $GdFe_2$ film exhibits the largest MCA energy of 14.1 meV and effective DMI of 1.6 meV. We attribute the substantial enhancement of MCA energy and DMI in $GdFe_2$ with the 5*d* capping layer to the strong SOC of the 5*d* orbitals because the SOC is proportional to the fourth power of the atomic number. Since the 4*d* also exhibit similar trend with 5*d*, Rh has the largest magnetic moments and MCA energy among other 4*d* TMs. This is related to the band-filling effect and orbital hybridization.

The calculated energy dispersion E(q) of spin spirals is presented in Figure 1 along the high-symmetry direction, $\bar{\Gamma}$-$\bar{K}$ for $GdFe_2$ capped by Rh and Ir which exhibit the largest magnetic moment, MCA energy, and effective DMI among the 4*d* and 5*d* TM elements, respectively. In the results without SOC, a minimum point of the energy dispersion is observed at the $\bar{\Gamma}$ point, and it degenerates for right-($q > 0$) and left-rotating ($q < 0$) spirals. For both Rh- and Ir-capped films, it is confirmed that the out-of-plane direction is an easy magnetization axis due to SOC (see Figure 2a). As a result of imperfect inversion symmetry at the interface, the SOC for spin spirals derives DMI in system [33,34]. Therefore, DMI leads to non-collinear spin structures with the magnetic moments on

an oblique angle. In case of the inclusion of the DMI, the E(q) has the lowest value for a homogeneous cycloidal flat spin spiral state with a particular rotational sense [35]. As presented in Figure 1, an energy minimum of −0.50 meV/atom and −0.35 meV/atom compared to the ground magnetic state appears for a right-rotating spin spiral for $GdFe_2$ films with Rh and Ir capping, respectively.

A skyrmion can be considered to be an intermediate state between spin spiral state and ferromagnetic state in a magnetic material because it rises from the competition between the exchange interaction that is responsible for the ferromagnetic state and the anisotropic exchange that generates spin spiral behavior. To investigate the magnetic phase transitions in $GdFe_2$/Rh and $GdFe_2$/Ir under the external magnetic field at 0 K, we have performed atomistic spin-dynamics simulations using the model described by Equation (1). Using the parameters obtained from DFT, the magnetic phase diagrams is displayed in Figure 4a,b. For both films capped by Rh and Ir, the ground magnetic state is a spin spiral consistent with the energy minimum at zero applied magnetic field. However, for the film capped by Rh, the skyrmion lattice is energetically stable at a critical field value of ∼1.12 T, and this skyrmion lattice phase is changed to the ferromagnetic phase by a larger critical field value of ∼2.25 T. For the film capped by Ir, the skyrmion lattice emerges at relatively weak field of 0.75 T, and disappears for a large filed of ∼1.74 T.

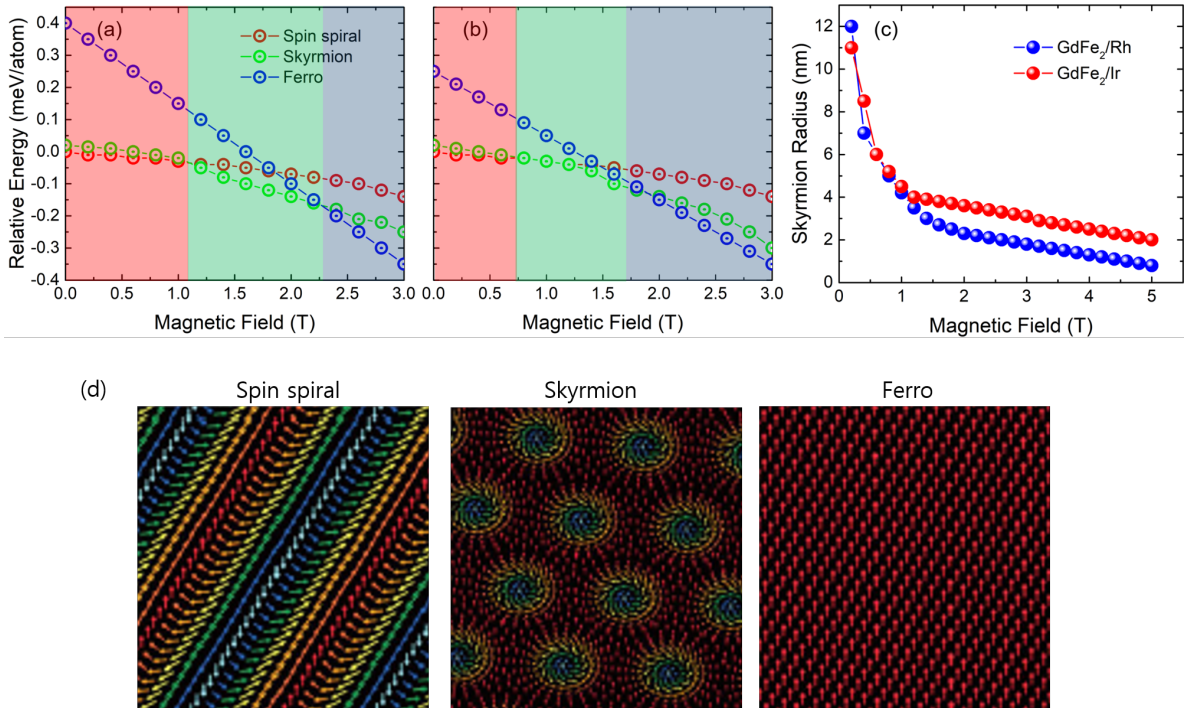

Figure 4. Phase diagrams for the (**a**) $GdFe_2$/Rh and the (**b**) $GdFe_2$/Ir films at zero temperature. The relative energies of the spin spiral states, skyrmion lattice, and ferromagnetic state are shown. The red, green, and blue colors represent the regime of the spin spiral states, skyrmion lattice, and ferromagnetic state, respectively. (**c**) Radii of skyrmions in the films of $GdFe_2$/Rh and $GdFe_2$/Ir as a function of the applied magnetic field. (**d**) Schematic representation of possible spin configurations in a magnetic material with Dzyaloshinsky–Moriya interaction for different values of an external field.

In our simulation, the spin structure is relaxed using spin dynamics. As shown in Figure 4c, skyrmions with a diameter of ∼2–4 nm emerge under external magnetic fields of 1–2 T for both Rh- and Ir-capped $GdFe_2$. The size of skyrmions decreases rapidly with the increasing value of applied magnetic field. For deeper insights into the skyrmion size, the diameter has been computed for isolated single skyrmions in two different ways: (i) Using the fixed MCA energy and exchange constants obtained from DFT calculation but varying the DMI value; (ii) using fixed DMI obtained from DFT

but varying the MCA. From these calculations we confirmed that the skyrmion size decreases with reduced DMI but it expands with reduced MCA.

4. Conclusions

The creation of extremely small, isolated and stabilized skyrmions of sizes of few nanometers in $GdFe_2$ films can be predicted by 4*d* and 5*d* TMs capping. While the atomistic spin model behavior was studied by spin dynamics simulations, first-principles parameters were obtained from density functional theory calculations. For future experimental work, this simulation work guides us in the exploration of novel skyrmion systems.

Author Contributions: conceptualization, S.J.; methodology, S.J. and A.D.; data curation, D.P. and X.Z.; writing draft, S.J., A.D., D.P., and X.Z.; project administration, S.J. and A.D.

Funding: This research was funded by ETH Zürich central funding.

Conflicts of Interest: The authors declare no conflict of interest.

References

1. Fert, A.; Cros, V.; Sampaio, J. Skyrmions on the track. *Nat. Nanotechnol.* **2013**, *8*, 152. [CrossRef]
2. Wiesendanger, R. Nanoscale magnetic skyrmions in metallic films and multilayers: A new twist for spintronics. *Nat. Rev. Mater.* **2016**, *1*, 16044. [CrossRef]
3. Kiselev, N.; Bogdanov, A.; Schäfer, R.; Rößler, U. Chiral skyrmions in thin magnetic films: New objects for magnetic storage technologies? *J. Phys. D Appl. Phys.* **2011**, *44*, 392001. [CrossRef]
4. Bogdanov, A.N.; Yablonskii, D.A. Thermodynamically stable "vortices" in magnetically ordered crystals. The mixed state of magnets *Sov. Phys. JETP* **1989**, *68*, 101.
5. Bogdanov, A.; Hubert, A. Thermodynamically stable magnetic vortex states in magnetic crystals. *J. Magn. Magn. Mater.* **1994**, *138*, 255–269. [CrossRef]
6. Bogdanov, A.; Rößler, U. Chiral symmetry breaking in magnetic thin films and multilayers. *Phys. Rev. Lett.* **2001**, *87*, 037203. [CrossRef]
7. Mühlbauer, S.; Binz, B.; Jonietz, F.; Pfleiderer, C.; Rosch, A.; Neubauer, A.; Georgii, R.; Böni, P. Skyrmion lattice in a chiral magnet *Science* **2009**, *323*, 915.
8. Wilhelm, H.; Baenitz, M.; Schmidt, M.; Rößler, U.; Leonov, A.; Bogdanov, A. Precursor phenomena at the magnetic ordering of the cubic helimagnet FeGe. *Phys. Rev. Lett.* **2011**, *107*, 127203. [CrossRef]
9. Münzer, W.; Neubauer, A.; Adams, T.; Mühlbauer, S.; Franz, C.; Jonietz, F.; Georgii, R.; Böni, P.; Pedersen, B.; Schmidt, M.; et al. Skyrmion lattice in the doped semiconductor $Fe_{1-x}Co_xSi$. *Phys. Rev. B* **2010**, *81*, 041203. [CrossRef]
10. Yu, X.Z.; Kanazawa, N.; Onose, Y.; Kimoto, K.; Zhang, W.Z.; Ishiwata, S.; Matsui, Y.; Tokura, Y. Near room-temperature formation of a skyrmion crystal in thin-films of the helimagnet FeGe *Nat. Mater.* **2011**, *10*, 106.
11. Tonomura, A.; Yu, X.; Yanagisawa, K.; Matsuda, T.; Onose, Y.; Kanazawa, N.; Park, H.S.; Tokura, Y. Real-space observation of skyrmion lattice in helimagnet MnSi thin samples. *Nano Lett.* **2012**, *12*, 1673–1677. [CrossRef] [PubMed]
12. Heinze, S.; Von Bergmann, K.; Menzel, M.; Brede, J.; Kubetzka, A.; Wiesendanger, R.; Bihlmayer, G.; Blügel, S. Spontaneous atomic-scale magnetic skyrmion lattice in two dimensions. *Nat. Phys.* **2011**, *7*, 713. [CrossRef]
13. Romming, N.; Hanneken, C.; Menzel, M.; Bickel, J.E.; Wolter, B.; von Bergmann, K.; Kubetzka, A.; Wiesendanger, R. Writing and deleting single magnetic skyrmions. *Science* **2013**, *341*, 636–639. [CrossRef] [PubMed]
14. Romming, N.; Kubetzka, A.; Hanneken, C.; von Bergmann, K.; Wiesendanger, R. Field-dependent size and shape of single magnetic skyrmions. *Phys. Rev. Lett.* **2015**, *114*, 177203. [CrossRef] [PubMed]
15. Woo, S.; Litzius, K.; Krüger, B.; Im, M.Y.; Caretta, L.; Richter, K.; Mann, M.; Krone, A.; Reeve, R.M.; Weigand, M.; et al. Observation of room-temperature magnetic skyrmions and their current-driven dynamics in ultrathin metallic ferromagnets. *Nat. Mater.* **2016**, *15*, 501. [CrossRef] [PubMed]

16. Soumyanarayanan, A.; Raju, M.; Oyarce, A.G.; Tan, A.K.; Im, M.Y.; Petrović, A.P.; Ho, P.; Khoo, K.; Tran, M.; Gan, C.; et al. Tunable room-temperature magnetic skyrmions in Ir/Fe/Co/Pt multilayers. *Nat. Mater.* **2017**, *16*, 898. [CrossRef] [PubMed]
17. Siemens, A.; Zhang, Y.; Hagemeister, J.; Vedmedenko, E.; Wiesendanger, R. Minimal radius of magnetic skyrmions: Statics and dynamics. *New J. Phys.* **2016**, *18*, 045021. [CrossRef]
18. Büttner, F.; Lemesh, I.; Beach, G.S. Theory of isolated magnetic skyrmions: From fundamentals to room temperature applications. *Sci. Rep.* **2018**, *8*, 4464. [CrossRef] [PubMed]
19. Jiang, W.; Zhang, X.; Yu, G.; Zhang, W.; Wang, X.; Jungfleisch, M.B.; Pearson, J.E.; Cheng, X.; Heinonen, O.; Wang, K.L.; et al. Direct observation of the skyrmion Hall effect. *Nat. Phys.* **2017**, *13*, 162. [CrossRef]
20. Litzius, K.; Lemesh, I.; Krüger, B.; Bassirian, P.; Caretta, L.; Richter, K.; Büttner, F.; Sato, K.; Tretiakov, O.A.; Förster, J.; et al. Skyrmion Hall effect revealed by direct time-resolved X-ray microscopy. *Nat. Phys.* **2017**, *13*, 170. [CrossRef]
21. Tomasello, R.; Martinez, E.; Zivieri, R.; Torres, L.; Carpentieri, M.; Finocchio, G. A strategy for the design of skyrmion racetrack memories. *Sci. Rep.* **2014**, *4*, 6784. [CrossRef] [PubMed]
22. Harris, V.G.; Pokhil, T. Selective-resputtering-induced perpendicular magnetic anisotropy in amorphous TbFe films. *Phys. Rev. Lett.* **2001**, *87*, 067207. [CrossRef] [PubMed]
23. Hansen, P.; Clausen, C.; Much, G.; Rosenkranz, M.; Witter, K. Magnetic and magneto-optical properties of rare-earth transition-metal alloys containing Gd, Tb, Fe, Co. *J. Appl. Phys.* **1989**, *66*, 756–767. [CrossRef]
24. Woo, S.; Song, K.M.; Zhang, X.; Zhou, Y.; Ezawa, M.; Liu, X.; Finizio, S.; Raabe, J.; Lee, N.J.; Kim, S.I.; et al. Current-driven dynamics and inhibition of the skyrmion Hall effect of ferrimagnetic skyrmions in GdFeCo films. *Nat. Commun.* **2018**, *9*, 959. [CrossRef] [PubMed]
25. Lee, J.T.; Chess, J.; Montoya, S.; Shi, X.; Tamura, N.; Mishra, S.; Fischer, P.; McMorran, B.; Sinha, S.; Fullerton, E.; et al. Synthesizing skyrmion bound pairs in Fe-Gd thin films. *Appl. Phys. Lett.* **2016**, *109*, 022402. [CrossRef]
26. Giannozzi, P.; Baroni, S.; Bonini, N.; Calandra, M.; Car, R.; Cavazzoni, C.; Ceresoli, D.; Chiarotti, G.L.; Cococcioni, M.; Dabo, I.; et al. QUANTUM ESPRESSO: A modular and open-source software project for quantum simulations of materials. *J. Phys. Cond. Matter* **2009**, *21*, 395502. [CrossRef]
27. Wimmer, E.; Krakauer, H.; Weinert, M.; Freeman, A.J. Full-potential self-consistent linearized-augmented-plane-wave method for calculating the electronic structure of molecules and surfaces: O_2 molecule *Phys. Rev. B* **1981**, *24*, 864. [CrossRef]
28. Kurz, P.; Förster, F.; Nordström, L.; Bihlmayer, G.; Blügel, S. Ab initio treatment of noncollinear magnets with the full-potential linearized augmented plane wave method. *Phys. Rev. B* **2004**, *69*, 024415. [CrossRef]
29. Eriksson, O.; Bergman, A.; Bergqvist, L.; Hellsvik, J. *Atomistic Spin Dynamics: Foundations and Applications*; Oxford University Press: Oxford, UK, 2017.
30. Antropov, V.P.; Katsnelson, M.I.; Harmon, B.N.; van Schilfgaarde, M.; Kusnezov, D. Spin dynamics in magnets: Equation of motion and finite temperature effects *Phys. Rev. B* **1996**, *54*, 1019. [CrossRef]
31. Katsnelson, M.I.; Irkhin, V.Y.; Chioncel, L.; Lichtenstein, A.I.; de Groot, R.A. Half-metallic ferromagnets: From band structure to many-body effects *Rev. Mod. Phys.* **2008**, *80*, 315. [CrossRef]
32. Vansteenkiste, A.; Leliaert, J.; Dvornik, M.; Helsen, M.; Garcia-Sanchez, F.; van Waeyenberge, B. The design and verification of MuMax3 *AIP Adv.* **2014**, *4*, 107133. [CrossRef]
33. Dzyaloshinskii, I.E. IE Dzyaloshinskii *Sov. Phys. JETP* **1957**, *5*, 1259.
34. Moriya, T. New mechanism of anisotropic superexchange interaction. *Phys. Rev. Lett.* **1960**, *4*, 228. [CrossRef]
35. Bode, M.; Heide, M.; Von Bergmann, K.; Ferriani, P.; Heinze, S.; Bihlmayer, G.; Kubetzka, A.; Pietzsch, O.; Blügel, S.; Wiesendanger, R. Chiral magnetic order at surfaces driven by inversion asymmetry. *Nature* **2007**, *447*, 190. [CrossRef] [PubMed]

© 2019 by the authors. Licensee MDPI, Basel, Switzerland. This article is an open access article distributed under the terms and conditions of the Creative Commons Attribution (CC BY) license (http://creativecommons.org/licenses/by/4.0/).